Parametric assessment of the effect of cochlear implant positioning on brain MRI artefacts at 3 Tesla

Short running head: MRI and CI location

RS Dewey 1,2,3, RA Dineen 1,3,4, M Clemence 5, O Dick 6, R Bowtell 1, PT Kitterick 2,3

1. Sir Peter Mansfield Imaging Centre, School of Physics and Astronomy, University of Nottingham, NG7 2RD, UK.
2. Hearing Sciences, Division of Clinical Neuroscience, School of Medicine, University of Nottingham, NG7 2UH, UK.
3. National Institute for Health Research (NIHR) Nottingham Biomedical Research Centre, Nottingham, NG1 5DU, UK.
4. Radiological Sciences, Division of Clinical Neuroscience, School of Medicine, University of Nottingham, NG7 2UH, UK.
5. Philips Healthcare, Best, Netherlands.
6. Radiology Department, Nottingham University Hospitals NHS Trust, Queens Medical Centre, Nottingham, NG7 2UH.

Address correspondence to: Rebecca Dewey; National Institute for Health Research (NIHR) Nottingham Biomedical Research Centre, Nottingham, UK. NG1 5DU; +441158232638; Rebecca.dewey@physics.org

Sources of support: This research was funded by the Nottingham Hospitals Charity grant and the infrastructure funding from the National Institute for Health Research. PTK's institution has received research grants from a manufacturer of cochlear implants, Cochlear Europe Ltd. The authors declare no other conflict of interest.

Acknowledgements

The authors would like to acknowledge Priya Archar at ENT Nottingham, Nottingham University Hospitals NHS Trust, Queen's Medical Centre, Nottingham, for her contribution of drawing the plausible implant locations on the silicone swimming cap while worn by one of the participants.

Parametric assessment of the effect of cochlear implant positioning on brain MRI artefacts at 3 Tesla

Abstract

Background: Brain magnetic resonance imaging (MRI) in patients with cochlear implants (CIs) is impacted by image artefacts.

Hypothesis: The optimal positioning of the CI to minimise artefacts is unknown. This study aimed to characterise the dependence of the extent and distribution of the artefact on CI positioning.

Methods: Three normally-hearing individuals underwent MRI using a standard T1-weighted 3D sequence. Scans were acquired with a non-functioning CI placed underneath a swimming cap at four plausible scalp positions on each side, and without the CI in situ. The artefact in each image was assessed quantitatively using voxel-based techniques. Two radiologists also independently rated the likely impact of the artefact on detection of pathology for 20 neuroradiological locations.

Results: The procedure was well tolerated. The most postero-inferior CI positions resulted in the smallest apparent artefacts. Radiological evaluations suggested that artefacts would likely limit pathology detection in the ipsilateral temporal, parietal and occipital lobes, regardless of CI location. Pathology detection in contralateral structures and anterior corpus callosum was rarely affected. Certain CI locations appeared to selectively spare ipsilateral structures, e.g., postero-inferior CI locations selectively spared ipsilateral midbrain, deep grey matter, and frontal lobes.

Conclusion: A CI placed under a swimming cap is a feasible tool for observing the effect of CI location on image usability within a single subject and potentially informing surgical planning. Regardless of CI placement, artefacts involving ipsilateral parietal, temporal and occipital lobes severely limited diagnostic image utility. Between 35% and 70% of neuroradiological features were deemed unaffected by the implant.

Hypothesis

The optimal positioning of the CI to minimise such artefacts is unknown. This study aimed to characterise the dependence of the extent and distribution of the CI artefact on CI positioning.

Introduction

Magnetic resonance imaging (MRI) forms a non-invasive imaging modality that is sensitive to many pathologies, and as such is often the preferred imaging technique for diagnosis and on-going disease evaluation. MRI is widely used in imaging diseases of the brain because the excellent soft tissue contrast and availability of a range of sequences that are sensitive to different pathological processes provide great diagnostic value. A cochlear implant (CI) is a device that provides auditory input for deaf individuals and comprises an implanted component (receiver-stimulator) and an external component (speech/sound processor) worn behind the ear. The implanted component contains a retaining magnet and a hermetically-sealed package with electronics placed under the scalp, and its presence raises MRI safety concerns [1], such as displacement of the internal retaining magnet and unintended acoustic stimulation [2].

Major manufacturers have revised the design of the implanted magnet to include a rotating component that minimises torque on the CI when it is placed in a magnetic field, thus improving patient comfort during MRI. However, clinical imaging of the head of CI-implanted patients is still confounded by substantial image artefacts caused by both the retaining magnet and the electronic components [3,4]. As a result, MRI is often avoided in this population. Computed tomography (CT) provides an alternative imaging technique that avoids the MRI-related safety concerns, but sensitivity to certain pathologies may not be as good as MRI, and image artefacts due to beam attenuation by the metallic components can also degrade CT images. Metal artefact reduction sequences (MARS) have recently been applied to spin-echo sequences on many scanner systems, but are associated with increased radiofrequency energy and consequently increased scan durations that could limit their utility in certain clinical settings [5].

Certain medical conditions associated with hearing loss may require regular (e.g. annual) MRI assessment to monitor disease progression. For example, neurofibromatosis type 2 (NF2), is a complex genetic condition that causes benign tumours (schwannomas) to grow along the nerves. Most commonly this affects the vestibular nerves, and while benign, vestibular schwannomas cause hearing loss for which cochlear implantation may be considered as a treatment when the cochlear nerve is anatomically preserved [6,7,8,9]. As annual monitoring of the brain is advised for people

with NF2 [10], the ability to safely acquire diagnostic-quality MRI in those with cochlear implants is important. A similar argument can be made for children with congenital disorders such as congenital cytomegalovirus infection or neurogenetic / mitochondrial disorders associated with deafness that may benefit from cochlear implantation [11,12,13], for which on-going MRI studies may be important for monitoring the associated brain disease. Furthermore, as cochlear implantation becomes widespread, MRI will become more important for diagnosing and monitoring unrelated, acquired brain pathologies in CI-implanted patients.

Removal of the retaining magnet is an effective method of reducing image artefacts due to CIs [14,15]. However, this approach requires the patient to undergo additional surgical procedures before and after each scan and may impose a period of auditory deprivation while wounds heal. Non-invasive methods of minimising the CI artefact would therefore significantly minimise patient burden in cases where regular brain MRI is indicated and address potential barriers preventing this patient group from benefitting from MRI imaging. Both the position of the CI implantation site [16] and the orientation of the head in the MR scanner [17] affect which regions of the image are affected by artefact and which anatomical features are visible. This study aimed to develop an approach to allow the evaluation of CI artefacts as the position of the implantable component is varied parametrically across different scalp positions. We demonstrate the utility of using a non-functioning CI device placed at 8 plausible surgical positions on the scalp of healthy volunteers by evaluating the extent and distribution of the CI artefact, and its impact on the diagnostic quality of a T1-weighted structural brain MRI sequence.

Materials and Methods

Participants

No formal sample size calculations were performed owing to the exploratory nature of the study activities. Experimental procedures conformed to the World Medical Association's Declaration of Helsinki and were approved by the University Faculty of Medicine and Health Sciences Research Ethics Committee (reference: 460-2001). All participants gave written informed consent. Participants were 23, 30 and 34 years old. Two of the participants were female.

Image acquisition

MRI data were acquired on a Philips 3.0 T Achieva MR scanner (Philips Healthcare, Best, Netherlands) using a 32-channel SENSE head coil. The scanner provided the MR conditional requirements for the Cochlear CI 612 implant by imposing the indicated safe performance limits

(ScanWise Implant, Philips Healthcare). Data were collected using a standard 3D-T1-weighted acquisition, taken from the manufacturer's defaults, so that it would be analogous to what would be used in the clinical setting, and would ensure that the extent of the artefact was not underestimated. The sequence used a steady-state (fast-field echo; FFE) gradient echo (GE) acquisition at 1.5 mm isotropic spatial resolution, reconstructed to 1 mm isotropic; field of view of 240×240×160 mm^3, echo time (TE) of 1.52 ms; repetition time (TR) of 25 ms, flip angle = 30°; bandwidth = 285 Hz, and sensitivity encoding (SENSE) factor 1.6. A stack comprising 150 contiguous sagittal slices provided whole-head coverage. The acquisition had a SAR of 0.484 Wkg^{-1}, took 2 min 57 s and was repeated nine times on each participant (8 scans with implant in situ, 1 control scan).

Procedure

The non-functioning Cochlear™ CI612 was prepared for scanning by separating and electrically isolating the two protruding electrode arrays using electrical tape. CI positions were standardised across participants using an adult silicone swimming cap which had been marked in permanent ink by an experienced ENT surgeon to reflect four viable sites for surgical placement of the internal CI component on each side of the head. The participant was fitted with earplugs for the attenuation of acoustic noise, and asked to wear the swimming cap. The fit of the cap was checked and adjusted to ensure that the markings were symmetrical, i.e. that the centre line of the swimming cap exactly followed the nasion to inion line on the participant. A 10-20 positioning system was attempted, but the shape of the cap meant that there was very little margin for movement in the forward-backward pitch of the cap. The position of each implant site was checked and determined to be on the skull. The distance between the magnet and the outer ear canal was 8.5 cm, 9.5 cm, 7.5 cm, and 6.5 cm (Figure 1), using a procedure similar to Todt et al [16]. The participant was then made comfortable in the scanner and the first T1 FFE scan acquired as a control. Following this, the scanner bed was moved out of the scanner and the participant allowed to lift their head such that the CI 612 could be placed in the first drawn position underneath the swimming cap. At this point the participant was asked if they experienced any sensation around the area of the implant, and whether there was any discomfort, heating, vibration, or any other sensation associated with the implant. The participant was then asked to return to the same position/orientation as previously and the scanner bed was returned to the same position and a second T1 FFE scan acquired. This procedure was repeated for each of the eight CI positions producing a total of nine T1 FFE scans. Figure 1 shows the positions of the CI locations on the swim cap.

Image pre-processing and analysis

Image pre-processing was performed using Statistical Parametric Mapping (SPM) version 12 (Wellcome Trust Centre for Neuroimaging, UK) and in-house software coded in MATLAB. Motion correction was performed in SPM12 to counteract the effect of the participant's head position differing between each acquisition due to lifting and replacing the head while placing or moving the CI. To improve the efficacy of the motion correction, a weighting image was used such that the motion correction software favoured information from areas that were unaffected by the presence of the implant in any image. This weighting image was calculated by taking the sum of the eight images where the implant was present, then thresholding this at an image intensity of 5000 (approximately the maximum signal intensity in images unaffected by artefact).

The motion-corrected images were then warped into standardised MNI space (Montreal Neurological Institute, Montreal, Canada) using SPM's normalization tool. Co-registration between the individual participant space and MNI space was performed using each participant's control image acquired before the CI was placed under the swimming cap, generating a transformation matrix. This transformation matrix was subsequently applied to all other motion-corrected images on an individual basis.

Control images (i.e. those with no CI present) were then segmented using SPM's segmentation tool, which provides tissue masks of grey matter, white matter, cerebrospinal fluid (CSF), bone and scalp. For each participant, the components containing grey matter, white matter, CSF and bone were summed, and re-thresholded at 1, to provide a binary mask of the entire head, without any artefact present. Each artefact image was then thresholded at an image intensity of 100 (the approximate signal of the CSF in the ventricles) and multiplied by that subject's binary control mask to give a binary mask of each artefact. To account for the variation in head size between participants, the size of the artefact (number of voxels in this artefact image) was expressed as a percentage of the total intracranial volume (number of voxels in the control image).

Radiological evaluation of the diagnostic impact of artefacts

To evaluate the diagnostic implications of the induced artefacts, two clinical radiologists with experience in brain MRI evaluation rated the presence of the artefact and the likely impact on the detection of pathology independently for 20 radiological brain anatomical locations (Figure 4). Unprocessed images were viewed using the RadiAnt DICOM Viewer 2020.2 [18]. The radiologists was asked to evaluate each location for the likely impact of artefact on the ability to identify pathology according to the following scale four point scale: (0) very unlikely to miss any abnormality, (1) a

subtle abnormality would be missed, (2) a moderate abnormality would be missed, and (3) a gross abnormality would be missed. Artefacts were then classified as one or more of the following types: (a) signal drop-out; (b) signal pile-up; (c) banding (large signal losses in bands); (d) rippling (smaller signal losses in ripples); (e) spatial distortion/warping; or (f) other, for which a free text description could be provided by the rater.

To assess the image usability, the modal rating of impact on the identification of pathology attained for each position of the CI and each brain region was calculated across raters and then across participants.

Statistical analyses

Repeated-measures analysis of covariance (ANOVA) was used to compare relative artefact volumes between individuals and between the 8 CI positions separately using SPSS version 26 (IBM, NY, USA). To assess inter-rater agreement for the radiological evaluations, a quadratic-weighted Cohen's Kappa was used in MedCalc for Windows, version 19.5.3 (MedCalc Software, Ostend, Belgium).

Results

Safety and tolerability

Upon asking whether participants experienced any sensation at the site of the device during scanning, no participant stated any adverse effects from the presence of the implant in any position. They all reported being unaware of the presence of the device, with the exception that they reported feeling and/or hearing "clicking" from the rotating retaining magnet as the implant was moved from site to site, or the participant was moved in and out of the scanner, between scans.

Quantification of artefact for different CI locations

Image co-registration outputs reported that the average displacement from the control image was 5.9 mm, with the maximum being 17.7 mm. The greatest rotational displacement of any image from the control image was less than 0.2°. Figure 2 shows the extent of the CI artefact for each of the eight positions (4 left, 4 right), and the relative artefact size and overlap in each of the three participants (raw data in supplemental material). Figure 3 shows the relative size of the CI artefact as a percentage of the total head size, in voxels. The artefact in positions 4 and 5 (the most posterior locations) was the smallest by percentage of total head size, but artefact volumes did not differ significantly across the 8 locations ($F_{3,6} = 4.036$; $p = 0.069$). The side on which the implant was positioned did not significantly affect the size of the artefact ($F_{1,2} = 0.028$; $p = 0.882$).

Radiological evaluation of diagnostic impact of artefacts for different CI locations

There was statistically "substantial" inter-rater agreement (as signified by a Quadratic Weighted Cohen's κ of between 0.61 and 0.80) on the impact of artefacts on the diagnostic utility of the images from all three participants (See Table 1). Figure 4 shows the modal rating attributed to each brain region and each CI location across raters and participants, representing the severity of the degree to which the artefact impacts the usefulness of the images. As the position of the CI was moved from most anterior to most posterior (i.e. left-most to medial and right-most to medial, see Figure 1), the number of total regions that were rated as potentially obscuring either a moderate or gross abnormality was lowest for the most anterior and most posterior CI positions, and highest for the positions in the middle of the range. Temporal, occipital, and parietal regions ipsilateral to the implant were severely affected by the CI in any position, whereas the anterior corpus callosum was relatively unaffected by the CI in any position. The frontal lobe, hippocampus, deep grey matter, and midbrain ipsilateral to the CI, as well as the posterior corpus callosum, were less affected when the CI was placed in posterior-most positions. Conversely, the ipsilateral cerebellum, pons and medulla were less affected when the implant was placed in more anterior positions.

The likelihood of missing pathology was associated significantly with signal dropout, which occurred 30% of the time ($r = 0.71$, $p < 0.05$), signal pileup (prevalence = 26%; $r = 0.59$, $p < 0.05$), banding (prevalence = 12%; $r = 0.29$, $p < 0.05$), and distortion (prevalence = 2%; $r = 0.07$, $p < 0.05$). The presence of rippling (prevalence = 16%) was not found to be strongly correlated with the likelihood of missing pathology ($r = 0.03$; $p > 0.1$).

Discussion

The present work was motivated by the needs of patients who are implanted with a CI while having a known co-morbidity that would benefit from regular monitoring with MRI such as NF2. Surgical removal and reinsertion of the implant magnet may have a cumulative detrimental impact on the scalp in the region of the implant and will not be practicable to perform indefinitely. As demonstrated in these findings, there is significant inter-subject variation in the impact of the implant location on the image artefact. This may be due to (a) differences in CI placement, which were carefully controlled for in the procedure; (b) inter-subject anatomical differences, which would be accounted for by alignment of the images, but any transformation, such as that into MNI space, would emphasise any differences in head size; or (c) the impact on the excitation efficiency of small differences in the orientation of the participant's head (and therefore the implant) relative to the

scanner magnetic field, which were only somewhat accounted for by consistent placement of the participant in the scanner. This inter-subject variability highlights the need for future studies to consider such inter-subject variations and other sources of variability and demonstrates the utility and importance of addressing implant site on a per-subject basis. The selection of a surgical site based on pre-operative evaluation of artefact distribution as described here could have long-term benefits in allowing optimal imaging of certain brain regions without the need for regular surgical intervention. As demonstrated in the current study, a comprehensive assessment of surgical options can be performed within an hour by an appropriately trained radiographic technologist with no adverse effects on the patient.

While the current study suggests it may not be feasible to image temporal, occipital, and parietal regions ipsilateral to the CI in any position, anatomical locations contralateral to the CI were generally much less severely affected, and the anterior corpus callosum was relatively unaffected by the CI in any position. An effect of anterior versus posterior CI placement was also observed such that posterior positions for the CI were associated with the lowest levels of artefact affecting the ipsilateral frontal lobe, hippocampus, deep grey matter and midbrain, and this information could be useful for planning CI placement in the presence of known lesions at these sites. For example, if a pre-implantation patient has a frontal meningioma on the side of planned implantation, then the more posterior CI positions (4 or 5, depending on side) would be most appropriate to reduce the chance of artefacts limiting the MRI follow-up of the meningioma. Conversely, if a known lesion involves the ipsilateral cerebellum, pons, or medulla are to be monitored, then the CI should be positioned more anteriorly , as a lesser degree of artefact was observed in these anatomical areas with CI positions 1 and 8.

The current study used only one image type (a 3D-T1-weighted sequence acquired at 1.5 mm^3, with a TE of 1.52 ms and a bandwidth of 285 Hz) to allow demonstration of proof-of-principle for this approach while maintaining an acceptable scan duration. In clinical practice the choice of MRI sequences obtained will depend on indications for the scan, and therefore the impact of the artefact on the diagnostic quality of the scan will vary with sequence selection. The use of a single sequence in this work limits the generalisability of our findings, as does the choice to use a sequence that is not compatible with MARS [19] or additions such as SEMAC (slice encoding for metal artifact correction) [20], which have been shown to significantly reduce the extent of the artefact, and increase the proportion of images that are usable [5]. These design choices were made to keep the length of the scanning protocol (comprising nine repetitions of the chosen sequence) to a

reasonable total duration for participants. We plan to extend the current work to map the artefact distribution and impact on diagnostic quality for other diagnostic imaging sequences commonly used in clinical neuroimaging. For example, the internal auditory meatus and membranous inner ear structures are typically assessed using heavily T2-weighted high-resolution sequences employing balanced steady-state acquisition, such as (FIESTA) or constructive interference in steady state (CISS). In addition, when monitoring the growth of ipsilateral or contralateral vestibular schwannomas or other intracranial manifestations associated with NF2, such as meningiomas, T1-weighted images with and without the injection of gadolinium contrast are typically used. 3D sequences are often favoured for clinical brain imaging because they facilitate rapid imaging of the whole brain volume providing thin slices for post-acquisition multi-planar reformatting. However, 3D sequences and sequences with thick slices can be more vulnerable to magnetic field inhomogeneities, such as those induced by metal, evident in through-plane geometric distortions. For this reason, 2D sequences with thin slices and other MARS implementations may provide images with less distortion, but at great time penalty. More generally in clinical brain imaging, certain commonly used sequences such as echo planar based diffusion weighted imaging and GE-based susceptibility weighted imaging sequences are more substantially affected by artefacts induced by metallic implants. Understanding the distribution of CI-induced artefacts for these commonly used clinical sequences will be valuable when considering device placement for CI candidates who are likely to need follow-up MRI.

While the majority of patients who are CI users will be scanned at the lower field strength of 1.5 T, the present study was conducted using a 3.0 T scanner to demonstrate the approach using the new generation of CIs featuring retaining magnets that can be safely scanned at 3.0 T. The current study demonstrates the feasibility and utility of pre-operative surveys to inform surgical planning in patients where routine MRI acquisition is anticipated or indicated. As the procedures described in this article were well tolerated and presented no adverse effects in healthy volunteers, further development and evaluation of a clinical protocol for mapping CI-induced artefact in individual pre-implantation patients is warranted, including assessing the impact of head orientation on image quality.

Conclusion

This study observed the effect of CI location on image quality and usability, for a high bandwidth, short TE, T1-weighted FFE (GE) scan, while controlling for inter-individual anatomical differences by scanning individuals wearing a swim cap with a non-functional CI placed underneath. This approach

was well tolerated, and a similar method of investigation could be performed for clinical purposes in a candidate for CI surgery, prior to implantation, to inform surgical planning. While implant position did not affect the visibility of brain regions such as the frontal, temporal, and parietal lobes contralateral to the CI, it did impact other regions. Posterior CI positions should be favoured to preserve the ability to image the frontal lobe, hippocampus, deep grey matter, and midbrain ipsilateral to the CI, whereas anterior positions favour the ipsilateral cerebellum, pons, and medulla.

Abbreviations

FFE = fast-field echo; GE = gradient echo; IAM = internal auditory meatus; MRI = magnetic resonance imaging; NF2 = neurofibromatosis type 2

References

1. Tam YC, Lee JWY, Gair J, Jackson C, Donnelly NP, Tysome JR, Axon PR, Bance ML. Performing MRI Scans on Cochlear Implant and Auditory Brainstem Implant Recipients: Review of 14.5 Years Experience. Otol Neurotol. 2020 Jun;41(5):e556-e562. doi: 10.1097/MAO.0000000000002569.

2. Walton J, et al. MRI without magnet removal in neurofibromatosis type 2 patients with cochlear and auditory brainstem implants. Otol Neurotol. 2014 Jun;35(5):821-5.

3. Edmonson HA, et al. MR Imaging and Cochlear Implants with Retained Internal Magnets: Reducing Artifacts near Highly Inhomogeneous Magnetic Fields. Radiographics. 2018 Jan-Feb;38(1):94-106.

4. Talbot BS, Weinberg EP. MR Imaging with Metal-suppression Sequences for Evaluation of Total Joint Arthroplasty. Radiographics. 2016 Jan-Feb;36(1):209-25.

5. Shah S, Padormo F, Knott K, Thomson S, Conner S, Charles-Edwards G, Touska P. Imaging the Internal Acoustic Meatus (IAMs) of patients with cochlear implants in-situ using Slice Encoded Metal Artefact Reduction. Proceedings of the International Society for Magnetic Resonance in Medicine, 2020, abstract number 3411.

6. Tolisano AM, Baumgart B, Whitson J, Kutz JW Jr. Cochlear implantation in patients with neurofibromatosis type 2. Otol Neurotol. 2019 Apr;40(4):e381-e385. doi: 10.1097/MAO.0000000000002165

7. Lustig LR, Yeagle J, Driscoll CL, Blevins N, Francis H, Niparko JK. Cochlear implantation in patients with neurofibromatosis type 2 and bilateral vestibular schwannoma. Otol Neurotol. 2006 Jun;27(4):512-8. doi: 10.1097/01.mao.0000217351.86925.51. PMID: 16791043.

8. Tan H, Jia H, Li Y, Zhang Z, Zhu W, Cai Y, Wang Z, Wu H. Impact of cochlear implantation on the management strategy of patients with neurofibromatosis type 2. Eur Arch Otorhinolaryngol. 2018 Nov;275(11):2667-2674. doi: 10.1007/s00405-018-5127-9. Epub 2018 Sep 18. PMID: 30229456

9. Carlson ML, Breen JT, Driscoll CL, Link MJ, Neff BA, Gifford RH, Beatty CW. Cochlear implantation in patients with neurofibromatosis type 2: variables affecting auditory performance. Otol Neurotol. 2012 Jul;33(5):853-62. doi: 10.1097/MAO.0b013e318254fba5

10. Lloyd SK, Evans DG. Neurofibromatosis type 2 service delivery in England. Neurosurgery Volume 64, Issue 5 , November 2018 , Pages 375-380. Doi: 10.1016/j.neuchi.2015.10.006

11. Fletcher KT, Horrell EMW, Ayugi J, Irungu C, Muthoka M, Creel LM, Lester C, Bush ML. The Natural History and Rehabilitative Outcomes of Hearing Loss in Congenital Cytomegalovirus: A Systematic Review. Otol Neurotol. 2018 Aug;39(7):854-864. doi: 10.1097/MAO.0000000000001861

12. Busi M, Rosignoli M, Castiglione A, Minazzi F, Trevisi P, Aimoni C, Calzolari F, Granieri E, Martini A. Cochlear Implant Outcomes and Genetic Mutations in Children with Ear and Brain Anomalies. Biomed Res Int. 2015;2015:696281. doi: 10.1155/2015/696281.

13. Yamamoto N, Okuyama H, Hiraumi H, Sakamoto T, Matsuura H, Ito J. The Outcome of Cochlear Implantation for Mitochondrial Disease Patients With Syndromic Hearing Loss. Otol Neurotol. 2015 Sep;36(8):e129-33. doi: 10.1097/MAO.0000000000000817

14. Wieser S, Igerc I, Hausegger K, Eckel H. Worldwide 1st MED-EL Mi1200 SYNCHRONY cochlear implant magnet removal for MRI image artifact reduction. Otolaryngology Case Reports, Volume 9, November 2018, Pages 41-44. https://doi.org/10.1016/j.xocr.2018.11.002 .

15. Wagner F, Wimmer W, Leidolt L, Vischer M, Weder S, Wiest R, Mantokoudis G, Caversaccio MD. Significant Artifact Reduction at 1.5T and 3T MRI by the Use of a Cochlear Implant with Removable Magnet: An Experimental Human Cadaver Study. PLoS One. 2015 Jul 22;10(7):e0132483. doi: 10.1371/journal.pone.0132483. eCollection 2015. PMID: 26200775

16. Todt, Ingo; Rademacher, Grit; Mittmann, Philipp; Wagner, Jan; Mutze, Sven; Ernst, Arne. MRI Artifacts and Cochlear Implant Positioning at 3 T In Vivo. Otology & Neurotology: July 2015 - Volume 36 - Issue 6 - p 972-976. doi: 10.1097/MAO.0000000000000720

17. Ay N, Todt I, Sudhoff H. Effects of head position on cochlear implant MRI artifacts at 3 T in vivo. Laryngo-Rhino-Otol 2019; 98(S 02): S214. DOI: 10.1055/s-0039-1685662.

18. Medixant. RadiAnt DICOM Viewer [Software]. Version 2020.2. Jul 19, 2020. URL: https://www.radiantviewer.com

19. Olsen RV, et al. Metal artifact reduction sequence: early clinical applications. Radiographics. 2000 May-Jun;20(3):699-712.

20. Lu W, Pauly KB, Gold GE, Pauly JM, Hargreaves BA. SEMAC: Slice Encoding for Metal Artifact Correction in MRI. Magn Reson Med. 2009 Jul; 62(1): 66–76.

Figures

Figure 1: A photograph of the CI positions as drawn onto a swim cap by an ENT surgeon experienced in cochlear implantation. The CI was placed underneath each outline in turn for the acquisition of an MR image in each participant. [Permission to use the image has been obtained from the subject.]

Figure 2: Extent of the CI artefact for each of the eight positions. Artefact extent was used to form a binary mask. Coloured areas represent the number of participants (out of three) for whom that area was obscured by image artefact generated by the CI. Bottom row shows the mathematical union of all four positions on the left and right of the head, respectively. Images shown are in conventional view (i.e. from below) and in MNI space. See supplemental material for raw images.

Figure 3: The relative artefact size, in terms of the percentage of the total head size in each of the three participants and at each CI position. Positions 1 and 8 were the most anterior, positions 4 and 5 the most posterior. Red vertical bars represent the mean across three participants for each position.

Figure 4: Radiological evaluation of artefact; impact of artefact on likely detection of abnormalities for each of the 20 brain regions as shown by the modal rating across raters and participants. Higher values, and red shading, indicate higher likelihood of an abnormality being missed by radiological evaluation, whereas lower/blue indicates a comparatively low likelihood of missing pathology. It is worth noting that there was a mode 9 brain regions out of 20 (range 7 to 14) that were deemed unlikely to impact the identification of pathology across all CI locations.

Tables

Table 1: Absolute agreement between raters in terms of the number of disagreements with a difference of more than 1 point on the scale, and Quadratic-Weighted Cohen's κ with 95% confidence intervals. Percentage of disagreements based on a total number of 180 ratings (20 brain regions across 8 CI locations and the control image).

Parametric assessment of the effect of cochlear implant positioning on brain MRI artefacts at 3 Tesla

Abstract

Background: Brain magnetic resonance imaging (MRI) in patients with cochlear implants (CIs) is impacted by image artefacts.

Hypothesis: The optimal positioning of the CI to minimise artefacts is unknown. This study aimed to characterise the dependence of the extent and distribution of the artefact on CI positioning.

Methods: Three normally-hearing individuals underwent MRI using a standard T1-weighted 3D sequence. Scans were acquired with a non-functioning CI placed underneath a swimming cap at four plausible scalp positions on each side, and without the CI in situ. The artefact in each image was assessed quantitatively using voxel-based techniques. Two radiologists also independently rated the likely impact of the artefact on detection of pathology for 20 neuroradiological locations.

Results: The procedure was well tolerated. The most postero-inferior CI positions resulted in the smallest apparent artefacts. Radiological evaluations suggested that artefacts would likely limit pathology detection in the ipsilateral temporal, parietal and occipital lobes, regardless of CI location. Pathology detection in contralateral structures and anterior corpus callosum was rarely affected. Certain CI locations appeared to selectively spare ipsilateral structures, e.g., postero-inferior CI locations selectively spared ipsilateral midbrain, deep grey matter, and frontal lobes.

Conclusion: A CI placed under a swimming cap is a feasible tool for observing the effect of CI location on image usability within a single subject and potentially informing surgical planning. Regardless of CI placement, artefacts involving ipsilateral parietal, temporal and occipital lobes severely limited diagnostic image utility. Between 35% and 70% of neuroradiological features were deemed unaffected by the implant.

Hypothesis

The optimal positioning of the CI to minimise such artefacts is unknown. This study aimed to characterise the dependence of the extent and distribution of the CI artefact on CI positioning.

Introduction

Magnetic resonance imaging (MRI) forms a non-invasive imaging modality that is sensitive to many pathologies, and as such is often the preferred imaging technique for diagnosis and on-going disease evaluation. MRI is widely used in imaging diseases of the brain because the excellent soft tissue contrast and availability of a range of sequences that are sensitive to different pathological processes provide great diagnostic value. A cochlear implant (CI) is a device that provides auditory input for deaf individuals and comprises an implanted component (receiver-stimulator) and an external component (speech/sound processor) worn behind the ear. The implanted component contains a retaining magnet and a hermetically-sealed package with electronics placed under the scalp, and its presence raises MRI safety concerns [1], such as displacement of the internal retaining magnet and unintended acoustic stimulation [2].

Major manufacturers have revised the design of the implanted magnet to include a rotating component that minimises torque on the CI when it is placed in a magnetic field, thus improving patient comfort during MRI. However, clinical imaging of the head of CI-implanted patients is still confounded by substantial image artefacts caused by both the retaining magnet and the electronic components [3,4]. As a result, MRI is often avoided in this population. Computed tomography (CT) provides an alternative imaging technique that avoids the MRI-related safety concerns, but sensitivity to certain pathologies may not be as good as MRI, and image artefacts due to beam attenuation by the metallic components can also degrade CT images. Metal artefact reduction sequences (MARS) have recently been applied to spin-echo sequences on many scanner systems, but are associated with increased radiofrequency energy and consequently increased scan durations that could limit their utility in certain clinical settings [5].

Certain medical conditions associated with hearing loss may require regular (e.g. annual) MRI assessment to monitor disease progression. For example, neurofibromatosis type 2 (NF2), is a complex genetic condition that causes benign tumours (schwannomas) to grow along the nerves. Most commonly this affects the vestibular nerves, and while benign, vestibular schwannomas cause hearing loss for which cochlear implantation may be considered as a treatment when the cochlear nerve is anatomically preserved [6,7,8,9]. As annual monitoring of the brain is advised for people

with NF2 [10], the ability to safely acquire diagnostic-quality MRI in those with cochlear implants is important. A similar argument can be made for children with congenital disorders such as congenital cytomegalovirus infection or neurogenetic / mitochondrial disorders associated with deafness that may benefit from cochlear implantation [11,12,13], for which on-going MRI studies may be important for monitoring the associated brain disease. Furthermore, as cochlear implantation becomes widespread, MRI will become more important for diagnosing and monitoring unrelated, acquired brain pathologies in CI-implanted patients.

Removal of the retaining magnet is an effective method of reducing image artefacts due to CIs [14,15]. However, this approach requires the patient to undergo additional surgical procedures before and after each scan and may impose a period of auditory deprivation while wounds heal. Non-invasive methods of minimising the CI artefact would therefore significantly minimise patient burden in cases where regular brain MRI is indicated and address potential barriers preventing this patient group from benefitting from MRI imaging. Both the position of the CI implantation site [16] and the orientation of the head in the MR scanner [17] affect which regions of the image are affected by artefact and which anatomical features are visible. This study aimed to develop an approach to allow the evaluation of CI artefacts as the position of the implantable component is varied parametrically across different scalp positions. We demonstrate the utility of using a non-functioning CI device placed at 8 plausible surgical positions on the scalp of healthy volunteers by evaluating the extent and distribution of the CI artefact, and its impact on the diagnostic quality of a T1-weighted structural brain MRI sequence.

Materials and Methods

Participants

No formal sample size calculations were performed owing to the exploratory nature of the study activities. Experimental procedures conformed to the World Medical Association's Declaration of Helsinki and were approved by the University Faculty of Medicine and Health Sciences Research Ethics Committee (reference: 460-2001). All participants gave written informed consent. Participants were 23, 30 and 34 years old. Two of the participants were female.

Image acquisition

MRI data were acquired on a Philips 3.0 T Achieva MR scanner (Philips Healthcare, Best, Netherlands) using a 32-channel SENSE head coil. The scanner provided the MR conditional requirements for the Cochlear CI 612 implant by imposing the indicated safe performance limits

(ScanWise Implant, Philips Healthcare). Data were collected using a standard 3D-T1-weighted acquisition, taken from the manufacturer's defaults, so that it would be analogous to what would be used in the clinical setting, and would ensure that the extent of the artefact was not underestimated. The sequence used a steady-state (fast-field echo; FFE) gradient echo (GE) acquisition at 1.5 mm isotropic spatial resolution, reconstructed to 1 mm isotropic; field of view of 240×240×160 mm^3, echo time (TE) of 1.52 ms; repetition time (TR) of 25 ms, flip angle = 30°; bandwidth = 285 Hz, and sensitivity encoding (SENSE) factor 1.6. A stack comprising 150 contiguous sagittal slices provided whole-head coverage. The acquisition had a SAR of 0.484 Wkg^{-1}, took 2 min 57 s and was repeated nine times on each participant (8 scans with implant in situ, 1 control scan).

Procedure

The non-functioning Cochlear™ CI612 was prepared for scanning by separating and electrically isolating the two protruding electrode arrays using electrical tape. CI positions were standardised across participants using an adult silicone swimming cap which had been marked in permanent ink by an experienced ENT surgeon to reflect four viable sites for surgical placement of the internal CI component on each side of the head. The participant was fitted with earplugs for the attenuation of acoustic noise, and asked to wear the swimming cap. The fit of the cap was checked and adjusted to ensure that the markings were symmetrical, i.e. that the centre line of the swimming cap exactly followed the nasion to inion line on the participant. A 10-20 positioning system was attempted, but the shape of the cap meant that there was very little margin for movement in the forward-backward pitch of the cap. The position of each implant site was checked and determined to be on the skull. The distance between the magnet and the outer ear canal was 8.5 cm, 9.5 cm, 7.5 cm, and 6.5 cm (Figure 1), using a procedure similar to Todt et al [16]. The participant was then made comfortable in the scanner and the first T1 FFE scan acquired as a control. Following this, the scanner bed was moved out of the scanner and the participant allowed to lift their head such that the CI 612 could be placed in the first drawn position underneath the swimming cap. At this point the participant was asked if they experienced any sensation around the area of the implant, and whether there was any discomfort, heating, vibration, or any other sensation associated with the implant. The participant was then asked to return to the same position/orientation as previously and the scanner bed was returned to the same position and a second T1 FFE scan acquired. This procedure was repeated for each of the eight CI positions producing a total of nine T1 FFE scans. Figure 1 shows the positions of the CI locations on the swim cap.

Image pre-processing and analysis

Image pre-processing was performed using Statistical Parametric Mapping (SPM) version 12 (Wellcome Trust Centre for Neuroimaging, UK) and in-house software coded in MATLAB. Motion correction was performed in SPM12 to counteract the effect of the participant's head position differing between each acquisition due to lifting and replacing the head while placing or moving the CI. To improve the efficacy of the motion correction, a weighting image was used such that the motion correction software favoured information from areas that were unaffected by the presence of the implant in any image. This weighting image was calculated by taking the sum of the eight images where the implant was present, then thresholding this at an image intensity of 5000 (approximately the maximum signal intensity in images unaffected by artefact).

The motion-corrected images were then warped into standardised MNI space (Montreal Neurological Institute, Montreal, Canada) using SPM's normalization tool. Co-registration between the individual participant space and MNI space was performed using each participant's control image acquired before the CI was placed under the swimming cap, generating a transformation matrix. This transformation matrix was subsequently applied to all other motion-corrected images on an individual basis.

Control images (i.e. those with no CI present) were then segmented using SPM's segmentation tool, which provides tissue masks of grey matter, white matter, cerebrospinal fluid (CSF), bone and scalp. For each participant, the components containing grey matter, white matter, CSF and bone were summed, and re-thresholded at 1, to provide a binary mask of the entire head, without any artefact present. Each artefact image was then thresholded at an image intensity of 100 (the approximate signal of the CSF in the ventricles) and multiplied by that subject's binary control mask to give a binary mask of each artefact. To account for the variation in head size between participants, the size of the artefact (number of voxels in this artefact image) was expressed as a percentage of the total intracranial volume (number of voxels in the control image).

Radiological evaluation of the diagnostic impact of artefacts

To evaluate the diagnostic implications of the induced artefacts, two clinical radiologists with experience in brain MRI evaluation rated the presence of the artefact and the likely impact on the detection of pathology independently for 20 radiological brain anatomical locations (Figure 4). Unprocessed images were viewed using the RadiAnt DICOM Viewer 2020.2 [18]. The radiologists was asked to evaluate each location for the likely impact of artefact on the ability to identify pathology according to the following scale four point scale: (0) very unlikely to miss any abnormality, (1) a

subtle abnormality would be missed, (2) a moderate abnormality would be missed, and (3) a gross abnormality would be missed. Artefacts were then classified as one or more of the following types: (a) signal drop-out; (b) signal pile-up; (c) banding (large signal losses in bands); (d) rippling (smaller signal losses in ripples); (e) spatial distortion/warping; or (f) other, for which a free text description could be provided by the rater.

To assess the image usability, the modal rating of impact on the identification of pathology attained for each position of the CI and each brain region was calculated across raters and then across participants.

Statistical analyses

Repeated-measures analysis of covariance (ANOVA) was used to compare relative artefact volumes between individuals and between the 8 CI positions separately using SPSS version 26 (IBM, NY, USA). To assess inter-rater agreement for the radiological evaluations, a quadratic-weighted Cohen's Kappa was used in MedCalc for Windows, version 19.5.3 (MedCalc Software, Ostend, Belgium).

Results

Safety and tolerability

Upon asking whether participants experienced any sensation at the site of the device during scanning, no participant stated any adverse effects from the presence of the implant in any position. They all reported being unaware of the presence of the device, with the exception that they reported feeling and/or hearing "clicking" from the rotating retaining magnet as the implant was moved from site to site, or the participant was moved in and out of the scanner, between scans.

Quantification of artefact for different CI locations

Image co-registration outputs reported that the average displacement from the control image was 5.9 mm, with the maximum being 17.7 mm. The greatest rotational displacement of any image from the control image was less than 0.2°. Figure 2 shows the extent of the CI artefact for each of the eight positions (4 left, 4 right), and the relative artefact size and overlap in each of the three participants (raw data in supplemental material). Figure 3 shows the relative size of the CI artefact as a percentage of the total head size, in voxels. The artefact in positions 4 and 5 (the most posterior locations) was the smallest by percentage of total head size, but artefact volumes did not differ significantly across the 8 locations ($F_{3,6} = 4.036$; $p = 0.069$). The side on which the implant was positioned did not significantly affect the size of the artefact ($F_{1,2} = 0.028$; $p = 0.882$).

Radiological evaluation of diagnostic impact of artefacts for different CI locations

There was statistically "substantial" inter-rater agreement (as signified by a Quadratic Weighted Cohen's κ of between 0.61 and 0.80) on the impact of artefacts on the diagnostic utility of the images from all three participants (See Table 1). Figure 4 shows the modal rating attributed to each brain region and each CI location across raters and participants, representing the severity of the degree to which the artefact impacts the usefulness of the images. As the position of the CI was moved from most anterior to most posterior (i.e. left-most to medial and right-most to medial, see Figure 1), the number of total regions that were rated as potentially obscuring either a moderate or gross abnormality was lowest for the most anterior and most posterior CI positions, and highest for the positions in the middle of the range. Temporal, occipital, and parietal regions ipsilateral to the implant were severely affected by the CI in any position, whereas the anterior corpus callosum was relatively unaffected by the CI in any position. The frontal lobe, hippocampus, deep grey matter, and midbrain ipsilateral to the CI, as well as the posterior corpus callosum, were less affected when the CI was placed in posterior-most positions. Conversely, the ipsilateral cerebellum, pons and medulla were less affected when the implant was placed in more anterior positions.

The likelihood of missing pathology was associated significantly with signal dropout, which occurred 30% of the time ($r = 0.71$, $p < 0.05$), signal pileup (prevalence = 26%; $r = 0.59$, $p < 0.05$), banding (prevalence = 12%; $r = 0.29$, $p < 0.05$), and distortion (prevalence = 2%; $r = 0.07$, $p < 0.05$). The presence of rippling (prevalence = 16%) was not found to be strongly correlated with the likelihood of missing pathology ($r = 0.03$; $p > 0.1$).

Discussion

The present work was motivated by the needs of patients who are implanted with a CI while having a known co-morbidity that would benefit from regular monitoring with MRI such as NF2. Surgical removal and reinsertion of the implant magnet may have a cumulative detrimental impact on the scalp in the region of the implant and will not be practicable to perform indefinitely. As demonstrated in these findings, there is significant inter-subject variation in the impact of the implant location on the image artefact. This may be due to (a) differences in CI placement, which were carefully controlled for in the procedure; (b) inter-subject anatomical differences, which would be accounted for by alignment of the images, but any transformation, such as that into MNI space, would emphasise any differences in head size; or (c) the impact on the excitation efficiency of small differences in the orientation of the participant's head (and therefore the implant) relative to the

scanner magnetic field, which were only somewhat accounted for by consistent placement of the participant in the scanner. This inter-subject variability highlights the need for future studies to consider such inter-subject variations and other sources of variability and demonstrates the utility and importance of addressing implant site on a per-subject basis. The selection of a surgical site based on pre-operative evaluation of artefact distribution as described here could have long-term benefits in allowing optimal imaging of certain brain regions without the need for regular surgical intervention. As demonstrated in the current study, a comprehensive assessment of surgical options can be performed within an hour by an appropriately trained radiographic technologist with no adverse effects on the patient.

While the current study suggests it may not be feasible to image temporal, occipital, and parietal regions ipsilateral to the CI in any position, anatomical locations contralateral to the CI were generally much less severely affected, and the anterior corpus callosum was relatively unaffected by the CI in any position. An effect of anterior versus posterior CI placement was also observed such that posterior positions for the CI were associated with the lowest levels of artefact affecting the ipsilateral frontal lobe, hippocampus, deep grey matter and midbrain, and this information could be useful for planning CI placement in the presence of known lesions at these sites. For example, if a pre-implantation patient has a frontal meningioma on the side of planned implantation, then the more posterior CI positions (4 or 5, depending on side) would be most appropriate to reduce the chance of artefacts limiting the MRI follow-up of the meningioma. Conversely, if a known lesion involves the ipsilateral cerebellum, pons, or medulla are to be monitored, then the CI should be positioned more anteriorly , as a lesser degree of artefact was observed in these anatomical areas with CI positions 1 and 8.

The current study used only one image type (a 3D-T1-weighted sequence acquired at 1.5 mm^3, with a TE of 1.52 ms and a bandwidth of 285 Hz) to allow demonstration of proof-of-principle for this approach while maintaining an acceptable scan duration. In clinical practice the choice of MRI sequences obtained will depend on indications for the scan, and therefore the impact of the artefact on the diagnostic quality of the scan will vary with sequence selection. The use of a single sequence in this work limits the generalisability of our findings, as does the choice to use a sequence that is not compatible with MARS [19] or additions such as SEMAC (slice encoding for metal artifact correction) [20], which have been shown to significantly reduce the extent of the artefact, and increase the proportion of images that are usable [5]. These design choices were made to keep the length of the scanning protocol (comprising nine repetitions of the chosen sequence) to a

reasonable total duration for participants. We plan to extend the current work to map the artefact distribution and impact on diagnostic quality for other diagnostic imaging sequences commonly used in clinical neuroimaging. For example, the internal auditory meatus and membranous inner ear structures are typically assessed using heavily T2-weighted high-resolution sequences employing balanced steady-state acquisition, such as (FIESTA) or constructive interference in steady state (CISS). In addition, when monitoring the growth of ipsilateral or contralateral vestibular schwannomas or other intracranial manifestations associated with NF2, such as meningiomas, T1-weighted images with and without the injection of gadolinium contrast are typically used. 3D sequences are often favoured for clinical brain imaging because they facilitate rapid imaging of the whole brain volume providing thin slices for post-acquisition multi-planar reformatting. However, 3D sequences and sequences with thick slices can be more vulnerable to magnetic field inhomogeneities, such as those induced by metal, evident in through-plane geometric distortions. For this reason, 2D sequences with thin slices and other MARS implementations may provide images with less distortion, but at great time penalty. More generally in clinical brain imaging, certain commonly used sequences such as echo planar based diffusion weighted imaging and GE-based susceptibility weighted imaging sequences are more substantially affected by artefacts induced by metallic implants. Understanding the distribution of CI-induced artefacts for these commonly used clinical sequences will be valuable when considering device placement for CI candidates who are likely to need follow-up MRI.

While the majority of patients who are CI users will be scanned at the lower field strength of 1.5 T, the present study was conducted using a 3.0 T scanner to demonstrate the approach using the new generation of CIs featuring retaining magnets that can be safely scanned at 3.0 T. The current study demonstrates the feasibility and utility of pre-operative surveys to inform surgical planning in patients where routine MRI acquisition is anticipated or indicated. As the procedures described in this article were well tolerated and presented no adverse effects in healthy volunteers, further development and evaluation of a clinical protocol for mapping CI-induced artefact in individual pre-implantation patients is warranted, including assessing the impact of head orientation on image quality.

Conclusion

This study observed the effect of CI location on image quality and usability, for a high bandwidth, short TE, T1-weighted FFE (GE) scan, while controlling for inter-individual anatomical differences by scanning individuals wearing a swim cap with a non-functional CI placed underneath. This approach

was well tolerated, and a similar method of investigation could be performed for clinical purposes in a candidate for CI surgery, prior to implantation, to inform surgical planning. While implant position did not affect the visibility of brain regions such as the frontal, temporal, and parietal lobes contralateral to the CI, it did impact other regions. Posterior CI positions should be favoured to preserve the ability to image the frontal lobe, hippocampus, deep grey matter, and midbrain ipsilateral to the CI, whereas anterior positions favour the ipsilateral cerebellum, pons, and medulla.

Abbreviations

FFE = fast-field echo; GE = gradient echo; IAM = internal auditory meatus; MRI = magnetic resonance imaging; NF2 = neurofibromatosis type 2

References

1. Tam YC, Lee JWY, Gair J, Jackson C, Donnelly NP, Tysome JR, Axon PR, Bance ML. Performing MRI Scans on Cochlear Implant and Auditory Brainstem Implant Recipients: Review of 14.5 Years Experience. Otol Neurotol. 2020 Jun;41(5):e556-e562. doi: 10.1097/MAO.0000000000002569.

2. Walton J, et al. MRI without magnet removal in neurofibromatosis type 2 patients with cochlear and auditory brainstem implants. Otol Neurotol. 2014 Jun;35(5):821-5.

3. Edmonson HA, et al. MR Imaging and Cochlear Implants with Retained Internal Magnets: Reducing Artifacts near Highly Inhomogeneous Magnetic Fields. Radiographics. 2018 Jan-Feb;38(1):94-106.

4. Talbot BS, Weinberg EP. MR Imaging with Metal-suppression Sequences for Evaluation of Total Joint Arthroplasty. Radiographics. 2016 Jan-Feb;36(1):209-25.

5. Shah S, Padormo F, Knott K, Thomson S, Conner S, Charles-Edwards G, Touska P. Imaging the Internal Acoustic Meatus (IAMs) of patients with cochlear implants in-situ using Slice Encoded Metal Artefact Reduction. Proceedings of the International Society for Magnetic Resonance in Medicine, 2020, abstract number 3411.

6. Tolisano AM, Baumgart B, Whitson J, Kutz JW Jr. Cochlear implantation in patients with neurofibromatosis type 2. Otol Neurotol. 2019 Apr;40(4):e381-e385. doi: 10.1097/MAO.0000000000002165

7. Lustig LR, Yeagle J, Driscoll CL, Blevins N, Francis H, Niparko JK. Cochlear implantation in patients with neurofibromatosis type 2 and bilateral vestibular schwannoma. Otol Neurotol. 2006 Jun;27(4):512-8. doi: 10.1097/01.mao.0000217351.86925.51. PMID: 16791043.

8. Tan H, Jia H, Li Y, Zhang Z, Zhu W, Cai Y, Wang Z, Wu H. Impact of cochlear implantation on the management strategy of patients with neurofibromatosis type 2. Eur Arch Otorhinolaryngol. 2018 Nov;275(11):2667-2674. doi: 10.1007/s00405-018-5127-9. Epub 2018 Sep 18. PMID: 30229456

9. Carlson ML, Breen JT, Driscoll CL, Link MJ, Neff BA, Gifford RH, Beatty CW. Cochlear implantation in patients with neurofibromatosis type 2: variables affecting auditory performance. Otol Neurotol. 2012 Jul;33(5):853-62. doi: 10.1097/MAO.0b013e318254fba5

10. Lloyd SK, Evans DG. Neurofibromatosis type 2 service delivery in England. Neurosurgery Volume 64, Issue 5 , November 2018 , Pages 375-380. Doi: 10.1016/j.neuchi.2015.10.006

11. Fletcher KT, Horrell EMW, Ayugi J, Irungu C, Muthoka M, Creel LM, Lester C, Bush ML. The Natural History and Rehabilitative Outcomes of Hearing Loss in Congenital Cytomegalovirus: A Systematic Review. Otol Neurotol. 2018 Aug;39(7):854-864. doi: 10.1097/MAO.0000000000001861

12. Busi M, Rosignoli M, Castiglione A, Minazzi F, Trevisi P, Aimoni C, Calzolari F, Granieri E, Martini A. Cochlear Implant Outcomes and Genetic Mutations in Children with Ear and Brain Anomalies. Biomed Res Int. 2015;2015:696281. doi: 10.1155/2015/696281.

13. Yamamoto N, Okuyama H, Hiraumi H, Sakamoto T, Matsuura H, Ito J. The Outcome of Cochlear Implantation for Mitochondrial Disease Patients With Syndromic Hearing Loss. Otol Neurotol. 2015 Sep;36(8):e129-33. doi: 10.1097/MAO.0000000000000817

14. Wieser S, Igerc I, Hausegger K, Eckel H. Worldwide 1st MED-EL Mi1200 SYNCHRONY cochlear implant magnet removal for MRI image artifact reduction. Otolaryngology Case Reports, Volume 9, November 2018, Pages 41-44. https://doi.org/10.1016/j.xocr.2018.11.002 .

15. Wagner F, Wimmer W, Leidolt L, Vischer M, Weder S, Wiest R, Mantokoudis G, Caversaccio MD. Significant Artifact Reduction at 1.5T and 3T MRI by the Use of a Cochlear Implant with Removable Magnet: An Experimental Human Cadaver Study. PLoS One. 2015 Jul 22;10(7):e0132483. doi: 10.1371/journal.pone.0132483. eCollection 2015. PMID: 26200775

16. Todt, Ingo; Rademacher, Grit; Mittmann, Philipp; Wagner, Jan; Mutze, Sven; Ernst, Arne. MRI Artifacts and Cochlear Implant Positioning at 3 T In Vivo. Otology & Neurotology: July 2015 - Volume 36 - Issue 6 - p 972-976. doi: 10.1097/MAO.0000000000000720

17. Ay N, Todt I, Sudhoff H. Effects of head position on cochlear implant MRI artifacts at 3 T in vivo. Laryngo-Rhino-Otol 2019; 98(S 02): S214. DOI: 10.1055/s-0039-1685662.

18. Medixant. RadiAnt DICOM Viewer [Software]. Version 2020.2. Jul 19, 2020. URL: https://www.radiantviewer.com

19. Olsen RV, et al. Metal artifact reduction sequence: early clinical applications. Radiographics. 2000 May-Jun;20(3):699-712.

20. Lu W, Pauly KB, Gold GE, Pauly JM, Hargreaves BA. SEMAC: Slice Encoding for Metal Artifact Correction in MRI. Magn Reson Med. 2009 Jul; 62(1): 66–76.

Figures

Figure 1: A photograph of the CI positions as drawn onto a swim cap by an ENT surgeon experienced in cochlear implantation. The CI was placed underneath each outline in turn for the acquisition of an MR image in each participant. [Permission to use the image has been obtained from the subject.]

Figure 2: Extent of the CI artefact for each of the eight positions. Artefact extent was used to form a binary mask. Coloured areas represent the number of participants (out of three) for whom that area was obscured by image artefact generated by the CI. Bottom row shows the mathematical union of all four positions on the left and right of the head, respectively. Images shown are in conventional view (i.e. from below) and in MNI space. See supplemental material for raw images.

Figure 3: The relative artefact size, in terms of the percentage of the total head size in each of the three participants and at each CI position. Positions 1 and 8 were the most anterior, positions 4 and 5 the most posterior. Red vertical bars represent the mean across three participants for each position.

Figure 4: Radiological evaluation of artefact; impact of artefact on likely detection of abnormalities for each of the 20 brain regions as shown by the modal rating across raters and participants. Higher values, and red shading, indicate higher likelihood of an abnormality being missed by radiological evaluation, whereas lower/blue indicates a comparatively low likelihood of missing pathology. It is worth noting that there was a mode 9 brain regions out of 20 (range 7 to 14) that were deemed unlikely to impact the identification of pathology across all CI locations.

Tables

Table 1: Absolute agreement between raters in terms of the number of disagreements with a difference of more than 1 point on the scale, and Quadratic-Weighted Cohen's κ with 95% confidence intervals. Percentage of disagreements based on a total number of 180 ratings (20 brain regions across 8 CI locations and the control image).

Figure 1 (TIFF, PDF, Word Doc, PPT, or EPS files are acceptable)

Figure 2 (TIFF, PDF, Word Doc, PPT, or EPS files are acceptable)

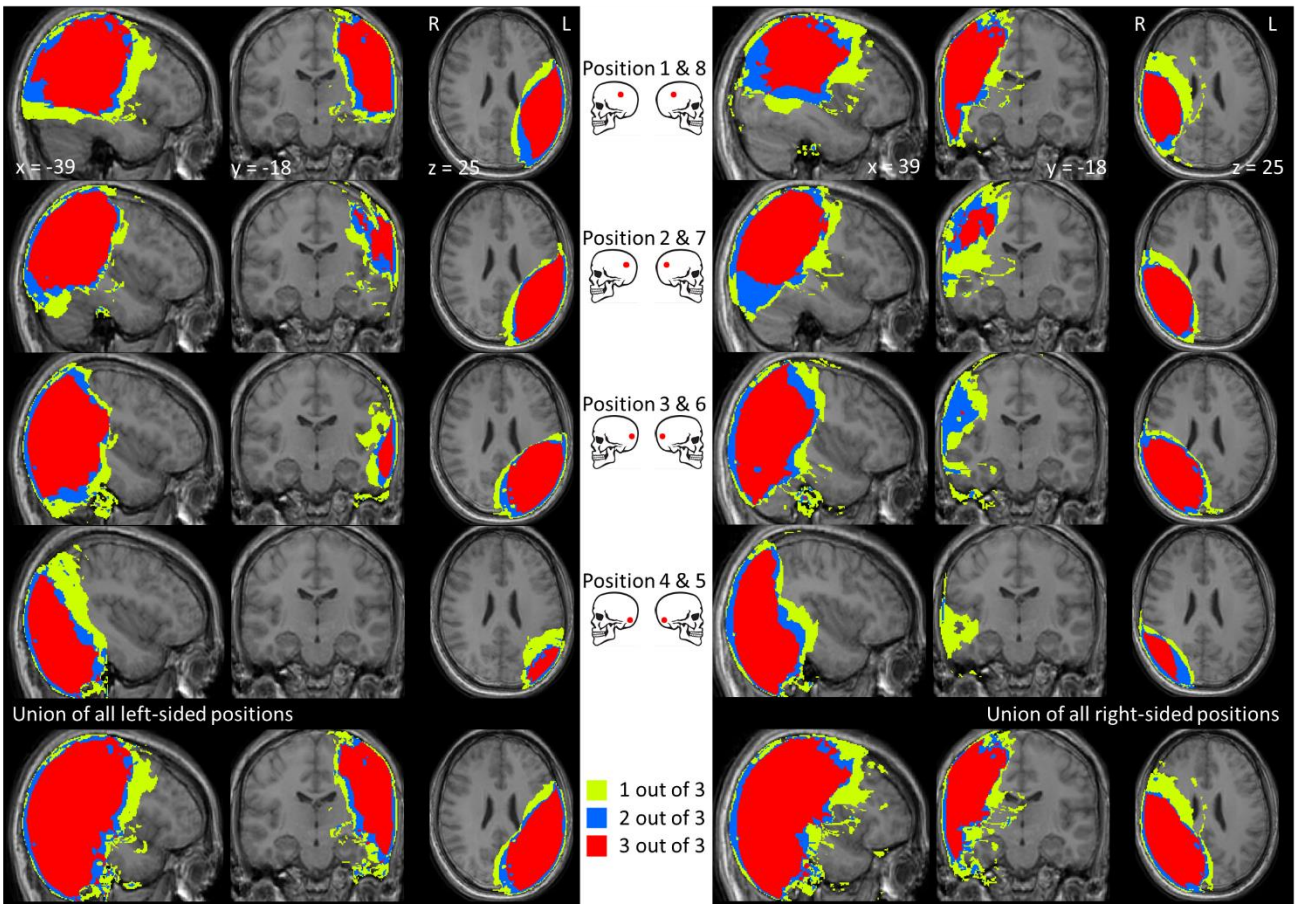

Figure 3 (TIFF, PDF, Word Doc, PPT, or EPS files are acceptable)

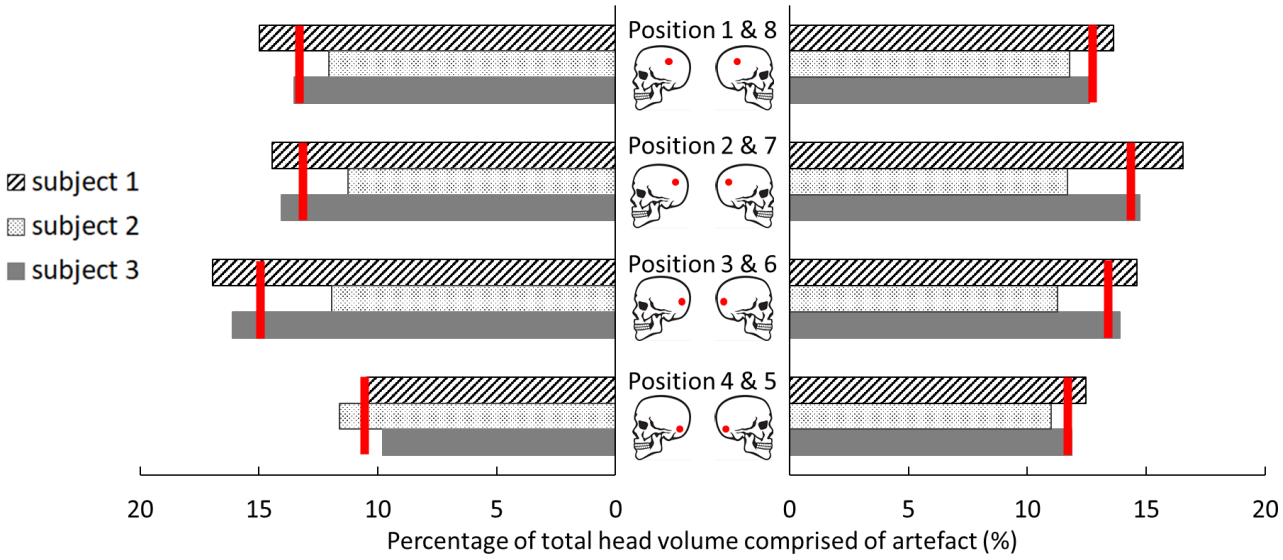

Figure 4 (TIFF, PDF, Word Doc, PPT, or EPS files are acceptable)

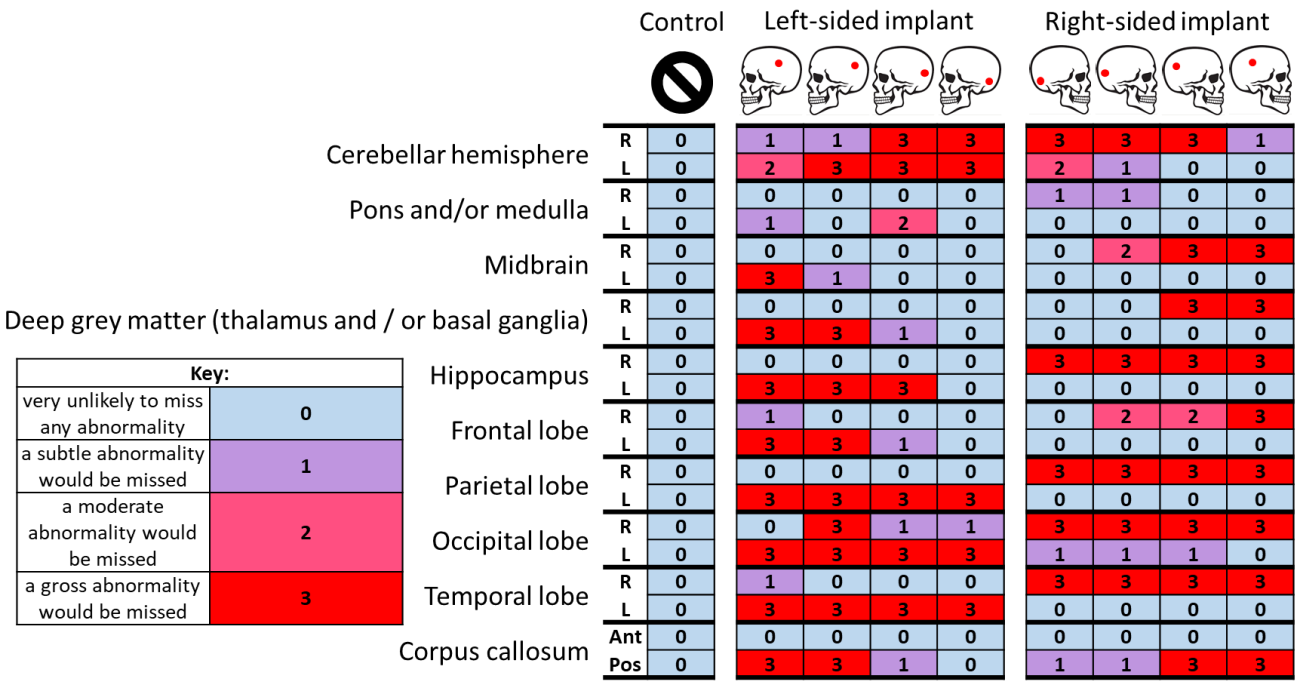

	Subject 1	Subject 2	Subject 3
Total agreements	75 % (n = 135)	73 % (n = 132)	77 % (n = 139)
Disagreements > 1 point	7 % (n = 12)	9 % (n = 16)	7 % (n = 12)
Quadratic-Weighted Cohen's κ	0.70	0.72	0.78
κ 95% confidence interval	0.63 - 0.76	0.66 - 0.78	0.74 - 0.83

Table 1: Absolute agreement between raters in terms of the number of disagreements with a difference of more than 1 point on the scale, and Quadratic-Weighted Cohen's κ with 95% confidence intervals. Percentage of disagreements based on a total number of 180 ratings (20 brain regions across 8 CI locations and the control image).